Spin-Echo Silencing Using a Current-Biased Frequency-Tunable Resonator

V. Ranjan,[1,*] Y. Wen,[2] A. K. V. Keyser,[1,3] S. E. Kubatkin,[4] A. V. Danilov,[4] T. Lindström,[1] P. Bertet,[2] and S. E. de Graaf[1,†]

[1]National Physical Laboratory, Teddington TW11 0LW, United Kingdom
[2]Université Paris-Saclay, CEA, CNRS, SPEC, 91191 Gif-sur-Yvette Cedex, France
[3]Imperial College London, Exhibition Road, SW7 2AZ, United Kingdom
[4]Department of Microtechnology and Nanoscience MC2, Chalmers University of Technology, SE-41296 Goteborg, Sweden

(Received 9 June 2022; revised 22 August 2022; accepted 6 October 2022; published 28 October 2022)

The ability to control microwave emission from a spin ensemble is a requirement of several quantum memory protocols. Here, we demonstrate such ability by using a resonator whose frequency can be rapidly tuned with a bias current. We store excitations in an ensemble of rare-earth ions and suppress on demand the echo emission ("echo silencing") by two methods: (1) detuning the resonator during the spin rephasing, and (2) subjecting spins to magnetic field gradients generated by the bias current itself. We also show that spin coherence is preserved during silencing.

DOI: 10.1103/PhysRevLett.129.180504

Electron spins are a leading platform for implementing quantum memories both in the optical [1–4] and microwave [5–7] domains, thanks to their long coherence times. Despite a relatively weak single spin-photon coupling, efficient absorption and emission of single photons [8,9] can be reached if the spin concentration is high enough to reach the high-cooperativity regime [10–21]. Moreover, the inhomogeneous broadening of the spin ensemble provides numerous orthogonal degrees of freedom to allow multimode storage of quantum states using protocols based on the Hahn echo [22–26].

Integrating a microwave multimode quantum memory with a superconducting processor holds promise in reducing physical qubit numbers by several orders of magnitude [27]. Such an architecture would benefit from arbitrary storage and retrieval of a desired quantum state. This, however, cannot be achieved with the conventional two-pulse Hahn echo sequence, since all stored states are simultaneously retrieved as last-in first-out. Moreover, the Hahn echo is emitted when the spins are all in the excited state, and thus, it unavoidably gets superimposed with noise coming from spin spontaneous emission [28,29].

To achieve dynamic control of storage times and avoid population inversion during retrieval, various methods have been proposed and experimentally explored. Controlled and reversible inhomogeneous broadening implemented with electric or magnetic field gradients [23,30], and cavity enhanced ac or dc Stark shifts [31–33] can delay the emission of excitations on demand. Alternatively, revival of silenced echo (ROSE) from double rephasing can be implemented with phase mismatching [29] or chirped pulses [34–36]. Recently, a modified ROSE protocol with refocusing pulses applied at frequencies different to input signals in a four-level Hilbert space, called noiseless photon echo (NLPE), has demonstrated low noise high-fidelity storage [37].

In this Letter, we investigate two ROSE-like methods of controlled suppression and retrieval of stored microwave fields by using current-biased fast frequency-tunable resonators (Fig. 1). The first method relies on the frequency tunability: after storage of an excitation and application of a refocusing pulse $\pi 1$, we rapidly detune the resonator during spin rephasing, thus, preventing the emission of an echo (referred throughout this Letter as "echo silencing" [38]). The detuning of the resonator is also useful for suppressing spin spontaneous emission by the Purcell effect [39–41] and, thus, for realizing a high-fidelity quantum memory. The second method uses the ability to pass a dc current

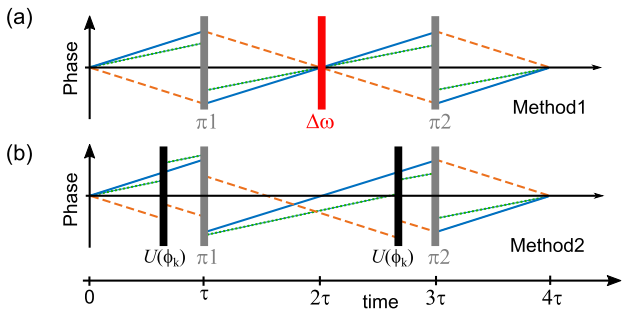

FIG. 1. The principle of revival of silenced echo (ROSE) [29] protocols to implement controlled suppression (at time $= 2\tau$) and retrieval (at time $= 4\tau$) of echoes by (a) fast detuning of the resonator frequency and (b) generating an inhomogeneous phase encoding on spins. The phase evolution of spins (only three plotted for clarity) are for a single excitation stored at time $= 0$, and the refocusing pulses $\pi 1$ and $\pi 2$ are ideal. Echo emission at 2τ is not desirable since it contains noise from spontaneously emitting spins excited by $\pi 1$.

through the resonator. The current generates a magnetic field gradient imparting an inhomogeneous, yet deterministic, unitary phase evolution $U(\phi_k)$ on the kth spin, such that spins do not rephase, and the echo is not formed [e.g., at time $= 2\tau$ in Fig. 1(b)]. In both methods, spin coherence is not affected by the act of echo silencing. Thus, spins continue to precess until a second refocusing pulse $\pi 2$ (preceded by an identical phase evolution U_k^{ϕ} in method 2) triggers the rephasing of spins and emission of an echo. The echo retrieved at time $= 4\tau$ avoids noise as spins are now in the ground state [29].

Our measurements are made possible by superconducting resonators made of NbN whose kinetic inductance (inductor width 2 μm and thickness 50 nm) allows for fast-tuning the resonance frequency ω_0 when a dc current I_{bias} is passed through it (see Ref. [42] and the Supplemental Material [43] for more details). The resonator performance is unaffected by the application of parallel magnetic fields up to 1 Tesla [48], which is necessary to bring spins in resonance. Previous work by Asfaw *et. al.* [49] with frequency tunable resonators explored multifrequency pulsed electron spin resonance experiments at a sample temperature of $T = 2$ K. In the following, we focus on aspects relevant to implementing a quantum memory, at 20 mK so that $\hbar\omega_0 \gg k_B T$.

The hybrid resonator-spin setup [Fig. 2(a)] is inductively coupled to a feedline with a rate $\kappa_c = 7.5 \times 10^3$ s^{-1}, through which microwave signals are sent and received in transmission. The total cavity decay rate $\kappa = \kappa_c + \kappa_i$ is dominated by κ_i, containing both dielectric losses and radiation losses through the current injection and exit terminals. We note that κ_i has input-power dependence due to the saturation of the two level system bath [42]. The resonator frequency varies quadratically with I_{bias} [bottom right of Fig. 2(a)], as expected from kinetic inductance changes [42,49,50]. The crystal containing spins is glued on the resonator with vacuum grease. Two configurations are used: in config. I, the crystal is placed in a region far from the path taken by the dc current, whereas in config. II the crystal is directly above the path of current flow [red dashed lines in Fig. 2(a)] and, thus, is maximally sensitive to magnetic field gradients.

The spins are provided by an ensemble of Er^{3+} ions in $CaWO_4$, with a nominal concentration 50 ppm (6.4×10^{17} cm^{-3}). Er^{3+} substituting Ca^{2+} ions in the lattice forms an effective electronic spin $S = 1/2$ system, with an anisotropic $\mathbf{g}$-tensor diagonal in the crystal frame ($g_{aa} = g_{bb} = 8.38$, $g_{cc} = 1.25$) [51,52]. Er^{3+} spin properties depend on the isotope: ^{167}Er has a nuclear spin $I = 7/2$ (with 23% abundance), while others have zero nuclear spin. Their spin Hamiltonians are $H_{\text{Er-167}}/\hbar = H_{\text{Er}}/\hbar - \mathbf{S}\cdot\mathbf{A}\cdot\mathbf{I} - \mu_n g_n \mathbf{B}\cdot\mathbf{I}$, and $H_{\text{Er}}/\hbar = \mu_B \mathbf{S}\cdot\mathbf{g}\cdot\mathbf{B}$, respectively. Here, $\mu_B(\mu_n)$ is Bohr (nuclear) magneton, $g_n = -0.162$ is the nuclear g factor [53], $\mathbf{B}$ the applied magnetic field vector, and $\mathbf{A}$ the hyperfine tensor,

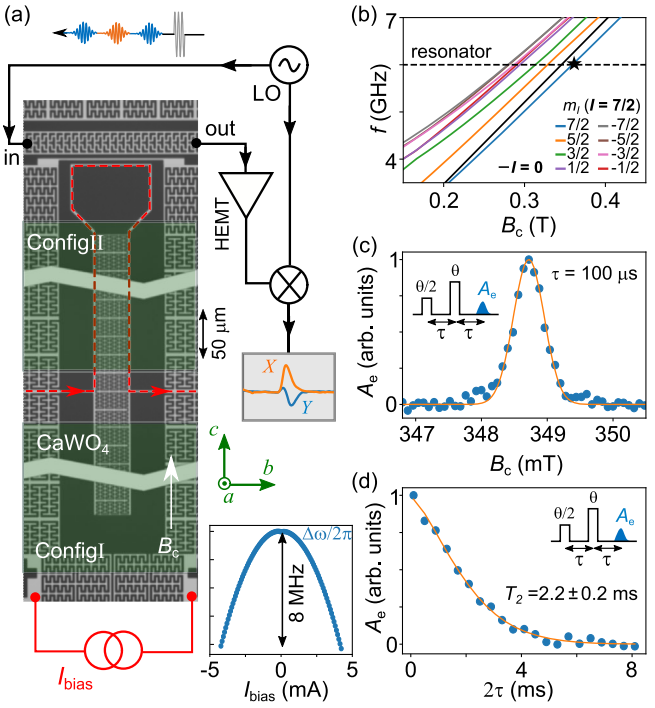

FIG. 2. Experimental setup. (a) An optical picture of the tunable resonator, the relative position of the $CaWO_4$ crystal, and a simplified measurement protocol. Horizontal zigzag discontinuities in the picture hide the long repetitive vertical features. Signal quadratures X, Y are measured in transmission of the feedline to which the resonator is inductively coupled. The injection and exit routes of the bias current I_{bias} are shown by the dashed red line. LO represents the local oscillator. Bottom right: the resonator frequency shift $\Delta\omega$ in response to I_{bias}. (b) Numerically calculated electron spin transition frequencies. $I = 0, 7/2$ refers to two Er isotopes, and m_I the nuclear-spin projection on the B-field axis. (c) Echo-detected spin spectroscopy and (d) decoherence (measured: symbols, fits: lines) at the transition with $m_I = 7/2$ as marked by the star in Fig. 2(b).

also diagonal in the crystal frame ($A_{aa}/2\pi = A_{bb}/2\pi = 870$ MHz, $A_{cc}/2\pi = 130$ MHz) [52,54]. Calculated electron spin transition frequencies for a magnetic field B_c aligned with the c axis are plotted in Fig. 2(b). In this Letter, we focus on the spin transition with nuclear spin projection on the B-field axis $m_I = 7/2$ marked by the star in Fig. 2(b), as it supports the longest spin coherence time (see Supplemental Material [43]).

Er^{3+} spins are probed either in continuous wave (Supplemental Material [43]) or with a pulsed Hahn-echo sequence ($\theta/2 - \tau - \theta - \tau -$ echo). Since spins are located everywhere in the crystal, they undergo largely inhomogeneous Rabi rotation angles under the rectangular-shaped microwave pulses used throughout this Letter (0.5 μs duration).

Echo-detected spectroscopy of the transition around 350 mT is plotted in Fig. 2(c). Here, and throughout, A_e represents the integrated area of the echo. We find an

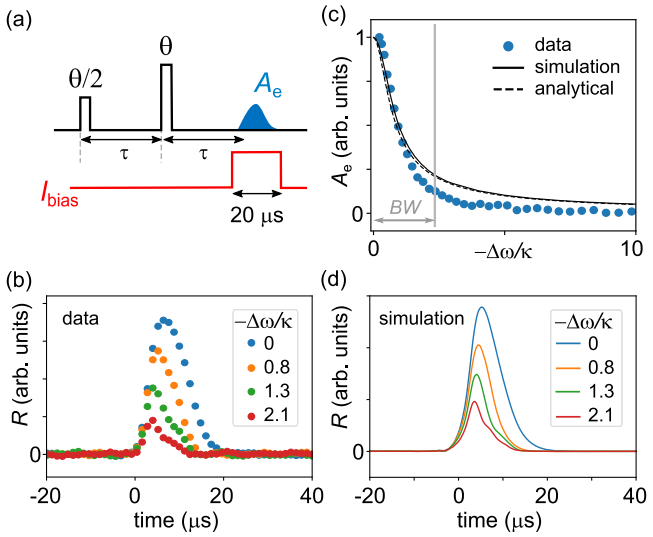

FIG. 3. Echo silencing with resonator tuning in config. I. (a) Measurement scheme. Square I_{bias} pulses of fixed duration 20 μs detune the resonator frequency by $\Delta\omega$ near the time of echo emission, $2\tau = 200$ μs. (b) Echo shapes for various detuning. R represents the signal magnitude $\sqrt{X^2+Y^2}$. (c) Measured (symbols) and numerically simulated (line) echo areas with increasing detuning. Measurement bandwidth (BW) is also shown. (d) Numerically simulated echo shapes.

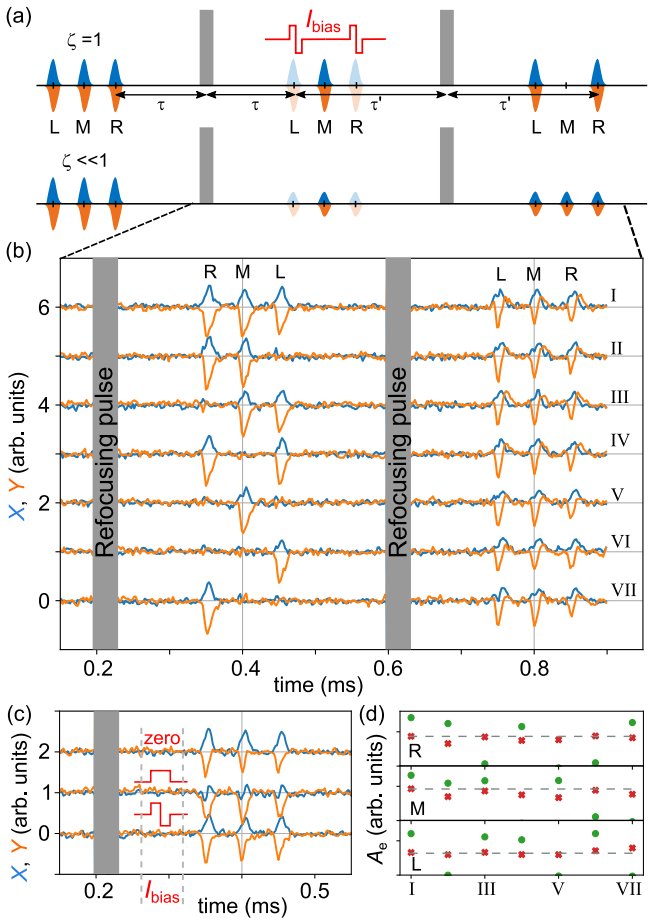

FIG. 4. Selective retrieval of microwave fields after a multimode storage. (a) Sketches of retrieval after storage of three identical input states for unit (top) and low (bottom) memory efficiency ζ using echo silencing by resonator detuning. Labels (L, M, and R) help identify the storage and rephasing times within the same memory mode. (b) Corresponding measured signal quadratures of retrieved states for different permutations of I_{bias} pulses. The I_{bias} pulses of amplitude 2 mA (yielding $-\Delta\omega/\kappa = 15$) and 20 μs total duration are made out of two halves of positive and negative current. The refocusing pulses are applied along the same axis. (c) Comparison of retrieved quadratures for cases when no I_{bias} (top) or 60 μs long I_{bias} pulses centered at time = 0.27 ms are applied with the same polarity (middle) or dual polarity (bottom) before the retrieval. (d) Area of retrieved echoes, primary as circles and secondary as crosses, for cases numbered in panel (b). Dashed horizontal lines represent signal magnitude of secondary echoes for case I with $I_{\mathrm{bias}} = 0$.

approximate Gaussian lineshape with a full width half maximum (FWHM) of 0.6 mT or $\Gamma/2\pi = 10.5$ MHz, which is much larger than the value due to dipolar couplings between spins for the nominal dopant concentration, ~200 kHz. This large broadening may arise from the inhomogeneous electric field caused by charge defects [55,56]. The echo magnitude A_e as a function of 2τ is shown in Fig. 2(e); its decay is fit with a stretched exponential $\exp[-(2\tau/T_2)^x]$ yielding $T_2 = 2.2$ ms and $x = 1.5$ [57]. Magnitude detection is employed to circumvent the phase noise from the experimental setup.

Now, we utilize the resonator frequency tunability to demonstrate echo silencing. Echo traces for I_{bias} pulses, of varying amplitude (yielding different detuning $\Delta\omega$) and fixed 20 μs duration applied around the time of echo emission [sketch in Fig. 3(a)], are plotted in Fig. 3(b). We observe a decrease of the echo magnitude with increased detuning. To analyze the spectral width of this decay, the echo area A_e is plotted as a function of the detuning $\Delta\omega$ normalized to the resonator linewidth κ, where we have taken the high-power $\kappa/2\pi = 0.14$ MHz. Numerical simulations assuming a uniform single spin-photon coupling strength g_0 are shown by solid line in Fig. 3(c), and semiquantitatively capture the decay. The discrepancy is due to limited bandwidth (BW) of the demodulation setup [58]. The simulated decay is well reproduced by the expression accounting for resonator filtering $[(\kappa/2)/\sqrt{\Delta\omega^2+\kappa^2/4}]$. The simulated echo shapes are plotted in Fig. 3(d), and show quantitative agreement with the experiment.

Having characterized the echo silencing, now, we demonstrate selective retrieval of microwave fields following their coherent multimode storage [22–26]. Three identical Gaussian pulses 50 μs apart and of FWHM = 4 μs (relative Rabi angle of $\pi/20$ and containing roughly 10^5 photons) are sent and retrieved using the Hahn echo protocol [Fig. 4(b)]. Different permutations of echo suppression with square $\pm I_{\mathrm{bias}}$ pulses (of total duration 20 μs,

with two equal halves of positive and negative current yielding $\Delta\omega = -15\kappa$) are applied across primary echoes (0.3 ms < time < 0.5 ms) to retrieve all, one, or two echoes at a time. The retrieved echo magnitudes and phases are not affected by the echo suppression preceding them, justifying that multiple coherences can be stored in orthogonal memory modes in a spin ensemble. Minor discrepancies can be attributed to the phase noise from the setup.

The I_{bias} pulses in Fig. 4(b) are made of two halves of positive and negative current to cancel the associated inhomogeneous magnetic field gradients (see Supplemental Material [43]). To show its importance, 60 μs long I_{bias} pulses are applied in between the refocusing pulse and echoes. As shown in Fig. 4(c), an I_{bias} pulse of single polarity induces a visible phase shift in the echo while the original echo phase is recovered when applying dual polarity.

To quantify the memory performance, the field retrieval efficiency of $\zeta = 7 \times 10^{-3}$ is obtained by comparing the integrated input fields with echoes (Supplemental Material [43]). This value is somewhat lower than the theoretical upper bound [8] $[4C/(1+C)(1-C)](\kappa_c/\kappa) = 1.1 \times 10^{-2}$ likely due to an inefficient refocusing pulse caused by spatially inhomogeneous Rabi angles. Here, the cooperativity $C = 4g_{\mathrm{ens}}^2/\kappa\Gamma = 0.23$ is deduced from continuous wave transmission spectroscopy yielding the ensemble coupling strength $g_{\mathrm{ens}}/2\pi = 0.35$ MHz. The low efficiency observed here is due to relatively large radiation losses through bias-current injection and exit terminals yielding a ratio $\kappa/\kappa_c \approx 100$ [43].

We also apply an identical second refocusing pulse to release the residual coherence stored in memory modes after being subjected to echo silencing. For comparison, we have plotted the echo magnitudes in Fig. 4(d). No visible changes, neither in the magnitude nor phase, are observed in secondary echoes (time > 0.7 ms) when corresponding primary echoes are suppressed. This is due to our low memory efficiency $\zeta \ll 1$, causing the emission of a stored state to be distributed over multiple spin refocusing cycles, in contrast to unit efficiency where a mode once allowed to emit will fully deplete the coherence stored within [Fig. 4(a)]. Thus, the final pursuit of arbitrary storage and retrieval based on echo-silencing protocol necessitates a high memory efficiency and efficient control pulses, such that same set of spins are rephased in different refocusing cycles.

Finally, we utilize the bias current I_{bias} as a local source of a magnetic field gradient on spins [23] to implement selective rephasing of spins needed for the ROSE protocol sketched in Fig. 1(b). To this end, we choose the crystal configuration (config. II). We note that strongly inhomogeneous Rabi angles, in addition to reducing memory efficiency, also lead to stimulated echoes (STEs) when more than two control pulses are involved. In the following, we limit our discussion to a basic demonstration of echo suppression and revival from field gradients, commonly known as gradient-recalled echoes in magnetic resonance spectroscopy [59].

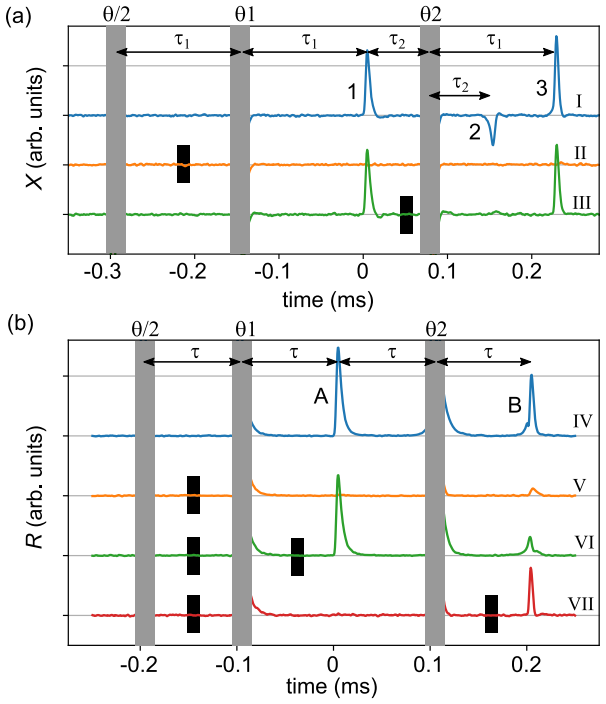

FIG. 5. Echo silencing with magnetic field gradients in config. II. (a) Signal quadrature of a train of echoes created by unevenly spaced control pulses. echo 1 (echo 2) is primary (secondary) rephasing of spin coherence created by $\theta/2$, echo 3 is three-pulse stimulated echo. (b) Signal magnitude of two echoes measured with even spacing of pulses. In both panels, each bias pulse is of single polarity, duration 20 μs and amplitude 3 mA (positions shown as black rectangles). The curves are vertically offset for clarity. All control pulses are applied along the same axis, with Rabi angles of $\theta = \theta 1 = \theta 2$.

Signal amplitudes after two cycles of refocusing and different positions of I_{bias} pulses are shown for uneven [Fig. 5(a)] and even [Fig. 5(b)] spacing of control pulses. From cases I and IV, measured without I_{bias} pulses, echo $1 \equiv$ echo A can be identified as primary rephasing of spin coherence created by $\theta/2$. Corresponding secondary rephasing (echo 2) and the three-pulse STE (echo 3) are temporally separated or together (echo $B \equiv$ echo 2 + echo 3). In cases II and V, a single I_{bias} pulse randomizes the coherence created by the $\theta/2$ pulse, and therefore, all echoes get suppressed. Overall suppression fidelity of the primary echo is $\mathcal{F} = 98 \pm 1\%$. In case III, the I_{bias} pulse only suppresses echo 2, leaving echo 3 intact. This is expected as STEs involve rephasing of longitudinal polarization grating of spins that do not precess [59,60], in contrast to normal spin echoes (e.g., echo 1, echo 2) that rephase transverse magnetization. As sketched in Fig. 1(b), a second I_{bias} pulse applied suitably should be able to cancel the inhomogeneous broadening imparted to spins.

This is tested for transverse components of spins in case VI. We see almost full revival of echo A ($\mathcal{F} = 96 \pm 1\%$), though echo B is only partially recovered compared to echo 2 of case I ($\mathcal{F} = 52 \pm 4\%$). In case VII, the I_{bias} configuration does not allow rephasing of transverse magnetization [see Fig. 1(b)], though the longitudinal spin component is recovered with a $\mathcal{F} = 36 \pm 3\%$ compared to echo 3 of case I. The reduced revival fidelity for secondary echo and STEs is likely due to errors in pulse angle accumulating with more pulses.

In summary, we have demonstrated the use of a current biased tunable resonator for echo suppression and phase preserving retrieval of microwave fields in an ensemble of Er^{3+} spins. The observed low efficiency here, despite $C = 0.23$, is primarily due to the low coupling rate κ_c of our resonator. To reach unit efficiency, first, improved resonator designs mitigating radiation losses from crystal mounting must be targeted to operate near the desired regime of $\kappa_c \approx \kappa$. Then, ensemble cooperativity can be increased to one by optimal crystal coverage on the resonator [43]. Last, a spatially localized spin ensemble [61] or chirped control pulses [34] are needed to attain efficient refocusing pulses. The imperfections of refocusing pulses will also affect the inverted spin population and, hence, the spontaneous emission noise on the retrieved states. In this direction, the NLPE protocol [37], that avoids noise even for imperfect pulses by leaving the population in an excited state different from the stored signal, could be adopted in the microwave regime. Demonstrated echo-silencing sequences can be repeated with short delay τ between refocusing pulses to realize high fidelity and arbitrary retrieval from a multimode quantum memory.

We acknowledge the support of the UK government department for Business, Energy and Industrial Strategy through the UK national quantum technologies program. A. D. and S. K. acknowledge support from the Swedish Research Council (VR) (Grant Agreements No. 2020-04393 and No. 2019-05480). S. D. G. acknowledges support by the Engineering and Physical Sciences Research Council (EPSRC) (Grant No. EP/W027526/1).

*vishal.ranjan@npl.co.uk
†sebastian.de.graaf@npl.co.uk

[1] A. I. Lvovsky, B. C. Sanders, and W. Tittel, Nat. Photonics **3**, 706 (2009).
[2] M. P. Hedges, J. J. Longdell, Y. Li, and M. J. Sellars, Nature (London) **465**, 1052 (2010).
[3] N. Sinclair, E. Saglamyurek, H. Mallahzadeh, J. A. Slater, M. George, R. Ricken, M. P. Hedges, D. Oblak, C. Simon, W. Sohler, and W. Tittel, Phys. Rev. Lett. **113**, 053603 (2014).
[4] M. Businger, A. Tiranov, K. T. Kaczmarek, S. Welinski, Z. Zhang, A. Ferrier, P. Goldner, and M. Afzelius, Phys. Rev. Lett. **124**, 053606 (2020).
[5] M. Steger, K. Saeedi, M. L. W. Thewalt, J. J. L. Morton, H. Riemann, N. V. Abrosimov, P. Becker, and H.-J. Pohl, Science **336**, 1280 (2012).
[6] G. Wolfowicz, A. M. Tyryshkin, R. E. George, H. Riemann, N. V. Abrosimov, P. Becker, H.-J. Pohl, M. L. W. Thewalt, S. a. Lyon, and J. J. L. Morton, Nat. Nanotechnol. **8**, 561 (2013).
[7] A. Ortu, A. Tiranov, S. Welinski, F. Fröwis, N. Gisin, A. Ferrier, P. Goldner, and M. Afzelius, Nat. Mater. **17**, 671 (2018).
[8] M. Afzelius, N. Sangouard, G. Johansson, M. U. Staudt, and C. M. Wilson, New J. Phys. **15**, 065008 (2013).
[9] J. J. L. Morton and P. Bertet, J. Magn. Reson. **287**, 128 (2018).
[10] A. Imamoglu, Phys. Rev. Lett. **102**, 083602 (2009).
[11] Y. Kubo, F. R. Ong, P. Bertet, D. Vion, V. Jacques, D. Zheng, A. Dréau, J.-F. Roch, A. Auffeves, F. Jelezko, J. Wrachtrup, M. F. Barthe, P. Bergonzo, and D. Esteve, Phys. Rev. Lett. **105**, 140502 (2010).
[12] D. I. Schuster, A. P. Sears, E. Ginossar, L. DiCarlo, L. Frunzio, J. J. L. Morton, H. Wu, G. A. D. Briggs, B. B. Buckley, D. D. Awschalom, and R. J. Schoelkopf, Phys. Rev. Lett. **105**, 140501 (2010).
[13] E. Abe, H. Wu, A. Ardavan, and J. J. L. Morton, Appl. Phys. Lett. **98**, 251108 (2011).
[14] X. Zhu, S. Saito, A. Kemp, K. Kakuyanagi, S.-i. Karimoto, H. Nakano, W. J. Munro, Y. Tokura, M. S. Everitt, K. Nemoto, M. Kasu, N. Mizuochi, and K. Semba, Nature (London) **478**, 221 (2011).
[15] R. Amsüss, C. Koller, T. Nöbauer, S. Putz, S. Rotter, K. Sandner, S. Schneider, M. Schramböck, G. Steinhauser, H. Ritsch, J. Schmiedmayer, and J. Majer, Phys. Rev. Lett. **107**, 060502 (2011).
[16] V. Ranjan, G. de Lange, R. Schutjens, T. Debelhoir, J. P. Groen, D. Szombati, D. J. Thoen, T. M. Klapwijk, R. Hanson, and L. DiCarlo, Phys. Rev. Lett. **110**, 067004 (2013).
[17] S. Probst, H. Rotzinger, S. Wünsch, P. Jung, M. Jerger, M. Siegel, A. V. Ustinov, and P. A. Bushev, Phys. Rev. Lett. **110**, 157001 (2013).
[18] H. Huebl, C. W. Zollitsch, J. Lotze, F. Hocke, M. Greifenstein, A. Marx, R. Gross, and S. T. B. Goennenwein, Phys. Rev. Lett. **111**, 127003 (2013).
[19] A. J. Sigillito, H. Malissa, A. M. Tyryshkin, H. Riemann, N. V. Abrosimov, P. Becker, H.-J. Pohl, M. L. W. Thewalt, K. M. Itoh, J. J. L. Morton, A. A. Houck, D. I. Schuster, and S. A. Lyon, Appl. Phys. Lett. **104**, 222407 (2014).
[20] B. C. Rose, A. M. Tyryshkin, H. Riemann, N. V. Abrosimov, P. Becker, H.-J. Pohl, M. L. W. Thewalt, K. M. Itoh, and S. A. Lyon, Phys. Rev. X **7**, 031002 (2017).
[21] J. R. Ball, Y. Yamashiro, H. Sumiya, S. Onoda, T. Ohshima, J. Isoya, D. Konstantinov, and Y. Kubo, Appl. Phys. Lett. **112**, 204102 (2018).
[22] J. H. Wesenberg, A. Ardavan, G. A. D. Briggs, J. J. L. Morton, R. J. Schoelkopf, D. I. Schuster, and K. Mølmer, Phys. Rev. Lett. **103**, 070502 (2009).
[23] H. Wu, R. E. George, J. H. Wesenberg, K. Molmer, D. I. Schuster, R. J. Schoelkopf, K. M. Itoh, A. Ardavan, J. J. L. Morton, and G. A. D. Briggs, Phys. Rev. Lett. **105**, 140503 (2010).

[24] C. Grezes, B. Julsgaard, Y. Kubo, M. Stern, T. Umeda, J. Isoya, H. Sumiya, H. Abe, S. Onoda, T. Ohshima, V. Jacques, J. Esteve, D. Vion, D. Esteve, K. Molmer, and P. Bertet, Phys. Rev. X **4**, 021049 (2014).
[25] S. Probst, H. Rotzinger, A. V. Ustinov, and P. A. Bushev, Phys. Rev. B **92**, 014421 (2015).
[26] V. Ranjan, J. O'Sullivan, E. Albertinale, B. Albanese, T. Chanelière, T. Schenkel, D. Vion, D. Esteve, E. Flurin, J. J. L. Morton, and P. Bertet, Phys. Rev. Lett. **125**, 210505 (2020).
[27] É. Gouzien and N. Sangouard, Phys. Rev. Lett. **127**, 140503 (2021).
[28] B. Julsgaard, C. Grezes, P. Bertet, and K. Molmer, Phys. Rev. Lett. **110**, 250503 (2013).
[29] V. Damon, M. Bonarota, A. Louchet-Chauvet, T. Chanelière, and J.-L. L. Gouët, New J. Phys. **13**, 093031 (2011).
[30] B. Kraus, W. Tittel, N. Gisin, M. Nilsson, S. Kröll, and J. I. Cirac, Phys. Rev. A **73**, 020302(R) (2006).
[31] T. Zhong, J. M. Kindem, J. G. Bartholomew, J. Rochman, I. Craiciu, E. Miyazono, M. Bettinelli, E. Cavalli, V. Verma, S. W. Nam, F. Marsili, M. D. Shaw, A. D. Beyer, and A. Faraon, Science **357**, 1392 (2017).
[32] C. Liu, T.-X. Zhu, M.-X. Su, Y.-Z. Ma, Z.-Q. Zhou, C.-F. Li, and G.-C. Guo, Phys. Rev. Lett. **125**, 260504 (2020).
[33] I. Craiciu, M. Lei, J. Rochman, J. G. Bartholomew, and A. Faraon, Optica **8**, 114 (2021).
[34] J. O'Sullivan, O. W. Kennedy, K. Debnath, J. Alexander, C. W. Zollitsch, M. Šimėnas, A. Hashim, C. N. Thomas, S. Withington, I. Siddiqi, K. Mølmer, and J. J. L. Morton, arXiv:2103.11697 [Phys. Rev. X (to be published)].
[35] M. Bonarota, J. Dajczgewand, A. Louchet-Chauvet, J.-L. L. Gouët, and T. Chanelière, Laser Phys. **24**, 094003 (2014).
[36] M. M. Minnegaliev, K. I. Gerasimov, R. V. Urmancheev, S. A. Moiseev, T. Chanelière, and A. Louchet-Chauvet, AIP Conf. Proc. **1936**, 020012 (2018).
[37] Y.-Z. Ma, M. Jin, D.-L. Chen, Z.-Q. Zhou, C.-F. Li, and G.-C. Guo, Nat. Commun. **12**, 4378 (2021).
[38] B. Julsgaard and K. Mølmer, Phys. Rev. A **88**, 062324 (2013).
[39] E. M. Purcell, Phys. Rev. **69**, 681 (1946).
[40] A. Bienfait, J. Pla, Y. Kubo, X. Zhou, M. Stern, C.-C. Lo, C. Weis, T. Schenkel, D. Vion, D. Esteve, J. Morton, and P. Bertet, Nature (London) **531**, 74 (2016).
[41] C. Eichler, A. J. Sigillito, S. A. Lyon, and J. R. Petta, Phys. Rev. Lett. **118**, 037701 (2017).
[42] S. Mahashabde, E. Otto, D. Montemurro, S. de Graaf, S. Kubatkin, and A. Danilov, Phys. Rev. Appl. **14**, 044040 (2020).
[43] See Supplemental Material at http://link.aps.org/supplemental/10.1103/PhysRevLett.129.180504 for additional details on setup, experiments, and theory, which includes references [44–47].
[44] M. L. Dantec, Ph.D thesis, Université Paris-Saclay, 2022.
[45] G. H. Larson and C. D. Jeffries, Phys. Rev. **141**, 461 (1966).
[46] V. Ranjan, S. Probst, B. Albanese, A. Doll, O. Jacquot, E. Flurin, R. Heeres, D. Vion, D. Esteve, J. J. L. Morton, and P. Bertet, J. Magn. Reson. **310**, 106662 (2020).
[47] Y. S. Bai and M. D. Fayer, Phys. Rev. B **39**, 11066 (1989).
[48] S. E. d. Graaf, A. V. Danilov, A. Adamyan, T. Bauch, and S. E. Kubatkin, J. Appl. Phys. **112**, 123905 (2012).
[49] A. T. Asfaw, A. J. Sigillito, A. M. Tyryshkin, T. Schenkel, and S. A. Lyon, Appl. Phys. Lett. **111**, 032601 (2017).
[50] M. R. Vissers, J. Hubmayr, M. Sandberg, S. Chaudhuri, C. Bockstiegel, and J. Gao, Appl. Phys. Lett. **107**, 062601 (2015).
[51] A. Antipin, A. Katyshev, I. Kurkin, and L. Y. Shekun, Sov. Phys. Solid State USSR **10**, 468 (1968).
[52] B. G. Enrique, J. Chem. Phys. **55**, 2538 (1971).
[53] J. V. Rakonjac, Y.-H. Chen, S. P. Horvath, and J. J. Longdell, Phys. Rev. B **101**, 184430 (2020).
[54] A. Abragam and B. Bleaney, *Electron Paramagnetic Resonance of Transition Ions*, Oxford Classic Texts in the Physical Sciences (Oxford University Press, New York, 2012).
[55] W. B. Mims and R. Gillen, Phys. Rev. **148**, 438 (1966).
[56] M. L. Dantec, M. Rančić, S. Lin, E. Billaud, V. Ranjan, D. Flanigan, S. Bertaina, T. Chanelière, P. Goldner, A. Erb, R. B. Liu, D. Estève, D. Vion, E. Flurin, and P. Bertet, Sci. Adv. **7**, eabj9786 (2021).
[57] M. Rančić, M. L. Dantec, S. Lin, S. Bertaina, T. Chanelière, D. Serrano, P. Goldner, R. B. Liu, E. Flurin, D. Estève, D. Vion, and P. Bertet, Phys. Rev. B **106**, 144412 (2022).
[58] For all cases of resonator detuning, local oscillator frequency is unchanged during demodulation (6 dB bandwidth of 300 kHz).
[59] A. Schweiger and G. Jeschke, *Principles of Pulse Electron Paramagnetic Resonance* (Oxford University Press, New York, 2001).
[60] D. Burstein, Concepts Magn. Reson. **8**, 269 (1996).
[61] V. Ranjan, B. Albanese, E. Albertinale, E. Billaud, D. Flanigan, J. J. Pla, T. Schenkel, D. Vion, D. Esteve, E. Flurin, J. J. L. Morton, Y. M. Niquet, and P. Bertet, Phys. Rev. X **11**, 031036 (2021).